Akebono/Suprathermal Mass Spectrometer observations of low-energy ion outflow: Dependence on magnetic activity and solar wind conditions

C. M. Cully, E. F. Donovan, A. W. Yau, and G. G. Arkos

Department of Physics and Astronomy, Institute for Space Research, University of Calgary, Calgary, Alberta, Canada

Received 30 November 2001; revised 10 June 2002; accepted 30 September 2002; published 26 February 2003.

[1] We present observations by the Suprathermal Mass Spectrometer (SMS) on Akebono (EXOS-D) of ion outflow in the energy range from <1 to ~70 eV. These observations cover a unique region of phase space and present an opportunity to "tie together" observations from disparate satellites. Variation of the total hemispheric O^+ and H^+ outflow rates with solar radio flux (monitored by the Penticton $F_{10.7}$ index), with geomagnetic activity (monitored by the *Kp* index), and with solar wind parameters is discussed. Comparisons of $F_{10.7}$ and *Kp* trends to results from Polar and Dynamics Explorer-1 (DE-1) lead us to conclude that flows of H^+ in this low energy range are entirely sufficient to account for higher-energy flows at higher altitudes. On the other hand, we infer a substantial amount of O^+ at energies above 70 eV. Both H^+ and O^+ outflow rates in this range exhibit a strong correlation with the solar wind kinetic pressure, the solar wind electric field, and the variability in the interplanetary magnetic field (IMF) in the hour preceding. While these factors are also associated with increased geomagnetic activity (*Kp*), a separate, *Kp*-independent effect is also found, showing a correlation of ion outflow with solar wind density and an anticorrelation with solar wind velocity. *INDEX TERMS:* 2764 Magnetospheric Physics: Plasma sheet; 2736 Magnetospheric Physics: Magnetosphere/ionosphere interactions; 2744 Magnetospheric Physics: Magnetotail; 2760 Magnetospheric Physics: Plasma convection; 2463 Ionosphere: Plasma convection

Citation: Cully, C. M., E. F. Donovan, A. W. Yau, and G. G. Arkos, Akebono/Suprathermal Mass Spectrometer observations of low-energy ion outflow: Dependence on magnetic activity and solar wind conditions, *J. Geophys. Res.*, *108*(A2), 1093, doi:10.1029/2001JA009200, 2003.

1. Introduction

[2] The composition of magnetospheric plasma is determined by source and loss process associated both with the ionosphere and with the solar wind (see the review by *Hultqvist et al.* [1999], and references therein). Insofar as sources of plasma from the ionosphere are concerned, outflowing ions from high latitudes represent a significant and at times dominant contribution of low-energy (thermal) plasma to the magnetosphere, their total mass contribution being on the order of 1 kg/s [*Yau and André*, 1997]. It is clear that ion outflow will have a direct effect on magnetospheric plasma composition, and a consequent indirect effect on magnetospheric dynamics [see, e.g., *Chappel et al.*, 1987; *Delcourt et al.*, 1989]. Of particular importance is the ability of different regions of the ionosphere to populate magnetospheric plasma populations, the dependence of these source processes on solar wind and other drivers, and the possible effects of the heavy (particularly O+) ions on magnetospheric dynamics. Quantitative knowledge of the magnitude and spatial and temporal variation of ion outflows at all energies is required to address these issues.

0148-0227/03/2001JA009200$09.00

[3] For the most part, ion outflow processes in the high latitude ionosphere may be grouped into two categories: bulk ion flows with energies up to a few eV in which all of the ions acquire a bulk flow velocity, and ion energization processes where some fraction of the ions are energized to much higher energies. The former category includes the polar wind and thermal O^+ upflow from the topside auroral ionosphere. The latter category includes energetic ion beams and conics from tens of eV to a few (and occasionally tens of) keV. *André and Yau* [1997] discussed the source mechanisms of the various ion outflow processes, and *Yau and André* [1997] reviewed published reports on the source strengths of the respective processes. The majority of previous studies focused on the nature (angular and energy distribution) of the energetic ion outflows and the altitude dependence of their physical morphology.

[4] To date, quantitative studies of outflow rates of energetic ions (above 10 eV) and their dependence on magnetic and solar activities based on multiyear data sets include those using the Energetic Ion Composition Spectrometer (EICS) on Dynamics Explorer-1 [*Yau et al.*, 1985] and the TIMAS instrument on Polar [*Peterson et al.*, 2001]; both instruments cover the ion energy range of about 10 eV to 16 keV. Quantitative observations of bulk ion flows, particularly the polar wind velocities and fluxes, were

reported from the DE-1 Retarding Ion Mass Spectrometer (RIMS) [*Chandler et al.*, 1991; *Chandler*, 1995] and the Akebono Suprathermal Mass Spectrometer (SMS) [*Abe et al.*, 1993, 1996] for the near solar maximum period, and the Polar Thermal Ion Dynamics Experiment (TIDE) [*Su et al.*, 1998] for the near solar minimum period.

[5] *Norqvist et al.* [1998] separated ion outflow into three types based on simultaneously-observed wave and particle characteristics. They found that 95% of total O^+ upflow is associated with broadband low-frequency waves. A separate energization mechanism functions in the midnight and premidnight sector, and is associated with resonant energization near the lower hybrid frequency or by electromagnetic ion cyclotron waves.

[6] Many previous studies on the variability of ion outflows focused on the dependence of the outflow rate on the level of solar and/or magnetic activity as gauged by the *Kp*, Dst, AE and $F_{10.7}$ indices. Fewer studies dealt with the ion outflow as a function of solar wind parameters. This latter category includes studies on the interplanetary magnetic field (IMF) dependence of the upward polar wind ion flux as observed on Akebono [*Abe et al.*, 1996] and Polar [*Elliott et al.*, 2001], on the IMF influence on the spatial distribution of ion conics on Viking [*Øieroset et al.*, 1999] and Akebono [*Miyake et al.*, 2000], and on the effect of enhanced solar wind dynamic pressure on energetic ion flux [*Moore et al.*, 1999].

[7] The extended operation of SMS has provided a unique data set of low-energy (<1 eV to about 70 eV) ion outflow with which to study both the long-term, solar-activity-related variations and the short term, magnetic-activity-related variations of low-energy ion outflow. In this paper, we extend the previous analyses of *Abe et al.* [1993] and *Drakou et al.* [1997], and present statistical results of the dependence of low-energy ion outflow at altitudes between 6000 and 10,000 km on magnetic activity and solar wind conditions. The paper is organized as follows: We first discuss how the data were acquired, reduced and selected for analysis. We then explain our division of the polar ionosphere into regions, present the observed hemispheric ion outflow rates and analyze their dependencies on solar wind conditions using multiple statistical regression. From the regression analysis, we identify solar wind parameters that exhibit a significant statistical correlation with the ion outflow rate. Finally, we conclude with a comparison between our results and previously published work and a discussion of the physical significance of the identified correlations. In a companion paper [*Cully et al.*, 2003], we use the statistical results presented here to study the supply of ionospheric ions to the central plasma sheet, and discuss the possible role of these ions in substorms.

2. Data Reduction

[8] The data used in this study were collected by the Suprathermal Mass Spectrometer (SMS) onboard the Akebono (EXOS-D) satellite [*Whalen et al.*, 1990; *Yau et al.*, 1998]. Data are from the thermal ''fast-scan'' mode, wherein the instrument measures the flux of H^+, He^+, O^+ and one of He^{++} or O^{++} at 8 retarding potential steps between 0 and ~20 eV and 32 angular steps in the spin plane of the satellite. Such a scan is typically performed every second spin.

[9] For the present analysis, we converted the instrument counts into approximate differential flux values by using the measured energy-dependent instrument response function. We corrected the effects of spacecraft charging under the ''thin sheath'' approximation $KE_\perp = KE'_\perp - qV_{s/c}$, where $KE_\perp$ and $KE'_\perp$ are the kinetic energies of the particle at the entrance aperture and outside the spacecraft sheath, respectively. $V_{s/c}$ is the spacecraft potential estimated using the method of *Drakou et al.* [1997]. The resulting ''spin-plane distribution functions'' give the differential flux in the spin plane as a function of velocity.

[10] To place the measurements in the guiding center frame of reference, we subtracted the satellite (ram) velocity and perpendicular drift velocity ($\vec{V}_{\vec{E}\times\vec{B}}$). While the ram velocity can be obtained from orbital records, $\vec{V}_{\vec{E}\times\vec{B}}$ must be estimated from the data. To accomplish this, we constructed differential flux profiles orthogonal to the spin plane projection of $\vec{B}$. The profiles were summed together, and the peak of the resulting net profile was determined by fitting a Gaussian distribution and assumed to correspond to the perpendicular component of the spin plane projected $\vec{V}_{\vec{E}\times\vec{B}}$. If the distribution was not well approximated by a Gaussian, we found the peak using a simple moment estimation.

[11] The above procedure reliably determines $\vec{V}_{\vec{E}\times\vec{B}}$ in the direction orthogonal to the spin-plane projection of $\vec{B}$. Unfortunately, if the spin plane contains neither $\vec{B}$ nor $\vec{V}_{\vec{E}\times\vec{B}}$, there is a component of $\vec{V}_{\vec{E}\times\vec{B}}$ parallel to the spin plane projection of $\vec{B}$. Although this component cannot be estimated from the data, its magnitude must be less than $|\vec{V}_{\vec{E}\times\vec{B}}|\tan(\theta)$, where is θ the angle between $\vec{B}$ and the spin plane. By only using data with $\theta < 20°$ we obtain a typical RMS error of ~0.3 km/s, in comparison with typical parallel flow velocities near 3 km/s [*Abe et al.*, 1993]. Since the resulting error is about as likely to be downward as it is to be upward, the mean error is much smaller than this. The elimination of this error requires measurements outside of the spin plane, such as are obtained by imaging spectrometers.

[12] If $\theta < 20°$ then the field-aligned direction is contained within the detector field of view. Under the assumption that the distribution is gyrotropic, we then inferred the 3-dimensional velocity distribution function (VDF) by creating a figure of revolution of the ''spin-plane distribution function''. The differential flux was assumed to fill each sampled piece of velocity space uniformly. To facilitate the comparison of VDFs from a range of altitudes, we ''projected'' each VDF to a common altitude of 8000 km using conservation of the first adiabatic invariant and the assumption of constant particle kinetic energy (i.e. neglecting electric field effects).

[13] To characterize the amount of plasma leaving the ionosphere, two different quantities were calculated for each observation: the *net flux* and the *upward (unidirectional) flux*. The *upward flux* is the total number of upward-moving ions that cross a unit area in a unit time. In the northern hemisphere, the upward flux is defined as

$$J_u(m) = 2\pi \int \int_{\pi/2}^{\pi} j(m, E, \beta) \cos(\pi - \beta) \sin(\beta) \mathrm{d}\beta \, \mathrm{d}E \qquad (1)$$

where $j(m, E, \beta)$ is the observed differential flux, β is the pitch angle and E is the energy. J_u is always positive.

[14] The *net flux* is similar to the upward flux, except that the integration also includes most of the downward portion of the differential flux, and the sign is reversed:

$$\Phi(m) = -2\pi \iint_{\beta_{lc}}^{\pi} j(m, E, \beta) \cos(\pi - \beta) \sin(\beta) \mathrm{d}\beta \, \mathrm{d}E \qquad (2)$$

The lower integration limit is set at the loss cone angle β_{lc} so that the net downward magnetospheric contribution is not included [*Yau et al.*, 1988; *Peterson et al.*, 2001]. In the northern hemisphere, negative values of Φ correspond to net outflow. Net flux is the quantity typically reported in the literature [*Yau and André*, 1997; *Norqvist et al.*, 1998; *Peterson et al.*, 2001], and is the total net number of ions leaving the ionosphere per unit area per unit time. It is distinct from the upward flux, which is simply the total number of ions moving up the field line per unit area per unit time.

3. Data Selection

[15] Between October 1989 and September 1998, there were a total of 504 480 records obtained between 6000 and 10,000 km in altitude, at geomagnetic latitudes above 60° in the northern hemisphere. Of these, 265 990 records were selected for the analysis based on the following criteria:

1. The entrance grid was biased at least 1 volt negative with respect to the ambient plasma.
2. The spin plane was no more than 20° from the magnetic field direction.
3. The nonlinear fitting algorithm of *Drakou et al.* [1997] converged to an estimate of the spacecraft charging either for the record itself or for the records surrounding it.

Of these criteria, item 2 resulted in the bulk of the rejected records.

[16] Several systematic bias and selection issues arise from the application of the above criteria. First, the satellite line of apsides drifts at a rate of 1 revolution every 18 months. The combination of the altitude requirement (near apogee) and the hemisphere requirement (Northern hemisphere) therefore means that data is taken in alternating 9-month periods. When combined with the fact that it takes 8 months for the orbital plane to precess to give a full scan of all local times, this makes the determination of seasonal trends subject to serious biasing problems.

[17] Second, the spacecraft charging is a function of density, being more severe in tenuous plasmas. The first criterion therefore preferentially selects high-density conditions. The number of records rejected for this reason was small (<1%).

[18] The second criterion, combined with the fact that the spin vector was Sun aligned, tends to reject records at lower latitudes near local noon and local midnight. This also introduces a slight selection bias in favor of observations taken during lower magnetic disturbance levels in these regions. The data is binned by position and usually by magnetic disturbance level in the analysis, so we do not consider this to be a significant issue. There is also a further seasonal bias introduced by this criterion.

[19] Finally, the fitting algorithm mentioned in the final criterion does not converge for very low densities, creating a bias toward higher density measurements. Very few records (<1%) were rejected on this basis. Overall, we have no reason to suspect serious problems with systematic biasing in the current analysis. Seasonal trends would require further work.

[20] Routine in-flight calibration operations have been performed over the course of the SMS lifetime in which the microchannel plate (MCP) bias voltage was varied rapidly and repeatedly from just below just below to just above the knee of the MCP response function while observing the ambient O+ intensity [*Whalen et al.*, 1990]. Measurements were thus made of: the MCP gain as a function of the bias voltage, the relative response between the 4 anode pixel columns and the 4 pixel rows of the MCP, and the mass response function of the instrument as a function of the radio-frequency voltage in its radio-frequency section. The routine calibration enables us to verify the continuing in-flight response of the instrument compared with the pre-flight calibration.

[21] Due to the abundance of thermal-energy ions, the lower-energy pixel columns have been struck by many more particles than their higher-energy counterparts. As anticipated over the course of the extended Akebono mission, the response of these pixels has degraded relative to the higher-energy pixel columns. The knee of the MCP response function has also shifted gradually to higher bias voltage, also as anticipated. To compensate for the gradually changing response of the instrument, the nominal operating voltage of the MCP was periodically adjusted upward to increase the gain of the MCP in the thermal "fast-scan" mode. The radio-frequency voltage in the radio-frequency section of the instrument was also adjusted on two occasions (in 1993 and 1996) to increase the energy gains of incident ions in the radio-frequency section and thereby deflect the ions away from the (relatively degraded) lower-energy pixel columns toward the higher-energy columns. The compensation scheme introduces uncertainties in the in-flight calibration of the instrument sensitivity, which is estimated to be about 30–40%.

4. Division of the Polar Ionosphere Into Regions

[22] For calculating the hemispheric outflow rates, measurements were sorted into 10 regions, as shown in Figure 1. The boundaries of the bins were defined by examination of upward flux values. The 10 regional bin boundary locations are functions of *Kp*, and generally correspond to known divisions of the ionosphere. Divisions are based on observed changes in the upward H^+ flux values, rather than on expectations of where these boundaries "should be". Differences between these boundaries and more commonly used ionospheric regions are primarily due to the high altitude of the observations.

[23] Using a parameter $s = 0.66\,Kp - 1$ to account for *Kp*-dependent motion of the auroral oval, we defined the invariant latitude boundaries to occur at $65 - s$, $72 - s$, $74 - s$ (for bin 5; see Figure 1), $81 + s$ and $83 + s$ (for bin 5). Magnetic local time borders occur at 0430, 0900, 1500 and 1930, except the division between bins 9 and 10, which is at 0600/1800. Although the morphology of H^+ and O^+ outflow is not exactly the same, very similar regions can be found in both data sets, and identical binning was used for both species. The minimum latitude of $65 - s$ is higher than many similar studies, leading to a somewhat smaller total area. However, data below this latitude were frequently

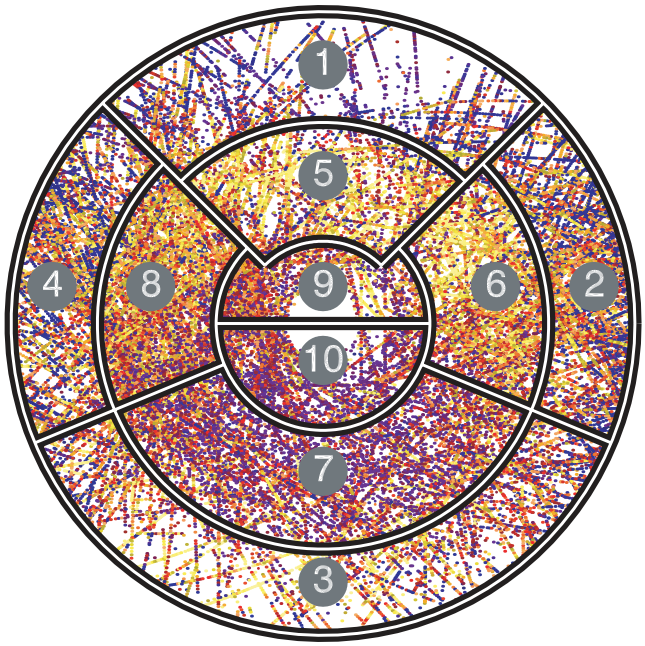

Figure 1. Polar cap regional boundaries for low *Kp* (<2). Points shown are color-coded observations of upward flux, and have invariant latitudes truncated at 85 degrees. Warmer colors indicate larger values of measured upward flux. The top of the figure is in the sunward direction, and the exact locations of the boundaries are described in the text. The low-latitude cutoff is roughly 65°.

found to be contaminated by the radiation belts, and were therefore deemed unusable.

[24] For each bin, we calculated the mean net outflow rate, also known as the *fluence*, by multiplying the area of the bin by the mean net flux observed within it. Areas of the (*Kp*-dependent) bins were calculated using the average *Kp* of all data used. Hemispheric fluence was calculated as the sum of all 10 bins. We also calculated the *upward fluence* by multiplying the bin areas by the respective mean upward fluxes.

5. Observations of Hemispheric Outflow as a Function of Magnetic Activity

[25] Terrestrial ion outflow rates are known to be well-correlated with both solar EUV (Extreme Ultraviolet Flux, represented by the proxy measurement $F_{10.7}$: the 10.7 cm radio flux measured at Penticton, Canada) and with different magnetic activity indices such as *Kp*, AE and Dst [*Yau et al.*, 1988; *Abe et al.*, 1996; *Yau and André*, 1997; *Peterson et al.*, 2001]. Although these relations have been discussed in previous studies, it is worthwhile to revisit this issue with the comprehensive data set that we have available. Additionally, the issue of upward fluence (distinct from net fluence) is infrequently discussed, and solar activity and magnetic activity trends are not known for this quantity.

[26] The essential difference between determining a relation between outflow and $F_{10.7}$ and doing the same for *Kp* is the timescale involved. $F_{10.7}$ responds very strongly to the solar cycle; at solar maximum, large fluctuations are present, with typical values in the range of 150 to 300, while at solar minimum, values are typically in the range 65 to 80 (units are 10^{-22} W m^{-2}Hz^{-1}). Since the instrument response changes more rapidly than the solar cycle, calibration problems are a more significant concern when fitting $F_{10.7}$ trends than when fitting *Kp* trends.

[27] Figure 2 is a plot of the hemispheric outflow rates as a function of $F_{10.7}$. All data were used in these graphs. Subsets of the data at high and low magnetic activity levels were also extracted and plotted in the same manner, yielding very similar curves offset by the expected amount. While the precise shape of these curves may be attributed to a large extent to time-dependent calibration uncertainties, we have no reason not to believe the overall trends: O^+ fluence increases by nearly 2 orders of magnitude over the full range of $F_{10.7}$, while H^+ increases only slightly, if at all. If a simple exponential dependence is assumed:

$$\begin{aligned} \Phi_{H^+} &\propto \exp(0.0088\ F_{10.7}) \\ J_{up,H^+} &\propto \exp(0.0074\ F_{10.7}) \\ \Phi_{O^+} &\propto \exp(0.034\ F_{10.7}) \\ J_{up,O^+} &\propto \exp(0.031\ F_{10.7}). \end{aligned} \tag{3}$$

Although a more complicated dependence may fit the data more closely, we feel that such a model is not justified in light of the calibration uncertainties. Uncertainties in the fitted coefficients are approximately 0.003. While this is a relatively small uncertainty for the O^+ fits, it is a substantial fraction of the H^+ coefficients.

[28] Our ability to study the dependence of fluence on magnetic activity is not subject to the same calibration related (instrument degradation) difficulties; all levels of magnetic activity occur during both solar maximum and solar minimum conditions. In order to examine the relationship between fluence and magnetic activity, we divided the data into two groups based on $F_{10.7}$. The low $F_{10.7}$ group included 114 185 data points with $F_{10.7}$ less than 100

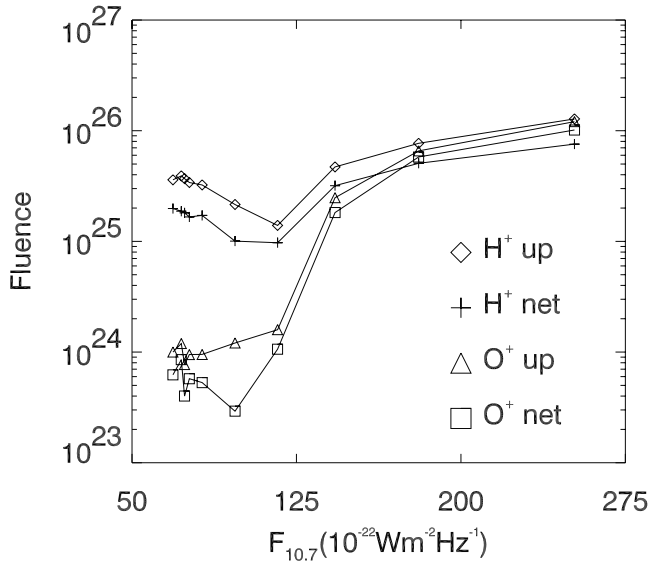

Figure 2. Fluence as a function of $F_{10.7}$. Data has been divided into 10 groups according to $F_{10.7}$, with an equal number of points in each group. The negative of net fluence is plotted.

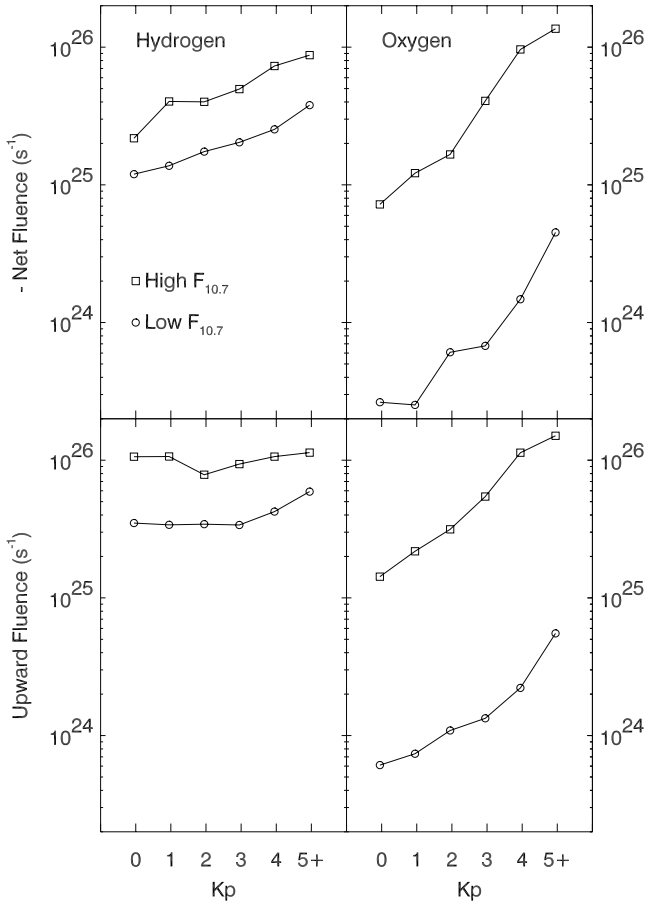

Figure 3. Dependence of hemispheric fluence and upward fluence on *Kp*. Top panels show net fluence values for H^+ (left) and O^+ (right). There is one line for each $F_{10.7}$ group. Bottom panels show upward fluences. All net fluences are negative, indicating net upward flow.

(average $F_{10.7}$ was 78, average *Kp* was 2); the high $F_{10.7}$ group (90 591 points) was defined as $F_{10.7} > 150$ (averages: $F_{10.7} = 205$, $Kp = 3+$). Figure 3 shows the dependence of the fluence on *Kp* for both groups.

[29] Variation of fluence with both EUV flux and magnetic activity is much more pronounced for O^+ than for H^+. The difference between fluences at solar minimum and solar maximum is roughly a factor of 20 for O^+, as opposed to a factor of 2 for H^+. As *Kp* varies from 0 to 5, the H^+ and O^+ net fluences vary by factors of ~4 and ~20, respectively. O^+ net fluence behaves nearly identically to the O^+ upward fluence, while H^+ net fluence is relatively independent of *Kp*.

[30] Since the *Kp* dependence does not seem to change substantially between the low and high $F_{10.7}$ groups, we felt it appropriate to fit the fluences with a curve of the form $F = a \exp[b\,Kp + cF_{10.7}]$. When such a fitting is done, the equations of best fit are:

$$\begin{aligned}
\Phi_{H^+} &= -6.6 \times 10^{24} \exp[0.0074F_{10.7} + 0.19Kp] \\
J_{up,H^+} &= 2.0 \times 10^{25} \exp[0.0045F_{10.7} + 0.11Kp] \\
\Phi_{O^+} &= -8.1 \times 10^{21} \exp[0.039F_{10.7} + 0.56Kp] \\
J_{up,O^+} &= 2.6 \times 10^{22} \exp[0.035F_{10.7} + 0.44Kp].
\end{aligned} \tag{4}$$

with uncertainties of ~0.003 and ~0.04 in the $F_{10.7}$ and *Kp* coefficients and ~30% in absolute magnitude.

6. Observations of Hemispheric Outflow as a Function of Solar Wind Parameters

[31] For questions concerning energy and momentum flow through the solar-terrestrial system, and for questions involving the eventual role of the outflowing ions within a dynamic magnetosphere, it is important to explore the statistical relation between solar wind properties and ion outflow. However, due to the large number of possibly relevant quantities, and their complicated interdependencies, this is not a straightforward task.

[32] Figure 4 consists of plots of the fluence as a function of a variety of different solar wind parameters. Solar wind data is from the Wind and IMP-8 satellites (using the OMNIWeb system of the National Space Science Data Center), available in hourly intervals and time-shifted to account for the delay between measurements at the satellite position and the time when that plasma reaches the magnetopause. Time shifting is described at http://nssdc.gsfc.nasa.gov/omniweb/html/addswe/addswe.html#2. The effects of $F_{10.7}$ on the fluences have been corrected by using formula 3 to normalize each individual flux value to the mean $F_{10.7}$ of 114. This decreased the magnitude of all of the trends, but was felt necessary for a meaningful comparison.

[33] The first row of Figure 4 begins with plots of fluence against solar wind density (left) and velocity (middle left). When considered independently, these trends are not exceptionally clear; however, the trend is quite apparent when the two are combined to calculate kinetic pressure, nmv^2 (middle right). H^+ net fluence seems to vary as strongly with solar wind kinetic pressure as it does with *Kp*, and its upward fluence, which shows little correlation with *Kp*, is also well-correlated with the kinetic pressure. O^+ net and upward fluences at the lowest pressures are an order of magnitude smaller than at the highest. The fluence is also well correlated with the kinetic energy flux, $\frac{1}{2}nmv^3$ (not shown). The rightmost plot on the top row is of fluence as a function of the direction of the solar wind velocity relative to the GSM equatorial plane, which we call the "latitude" of the flow vector. This angle is positive for flow from the south of the Sun. There seems to be some trend with this quantity, although it is difficult to ascertain exactly what it might be.

[34] The second row of Figure 4 begins with the dependence of hemispheric fluence on the solar wind electric field. The electric field has been calculated as $|E| = |v||B|\sin(\theta_{VB})$, where θ_{VB} is the angle between the hourly-averaged $\vec{v}$ and $\vec{B}$. The fluence is clearly larger for larger electric field strengths, a trend further supported by the near-sinusoidal relation with θ_{VB} shown in the second panel.

[35] Each solar wind value is the mean of between roughly 60 and 235 individual measurements. The standard deviations of the solar wind parameters in these measurements can also be calculated; for velocity (σ_v) and magnetic field (σ_B), this gives some idea of the turbulence and wave power in the solar wind on the timescale of several minutes. There is a strong positive correlation between these quantities and the fluence, as can be seen in the rightmost panels of the second row of Figure 4.

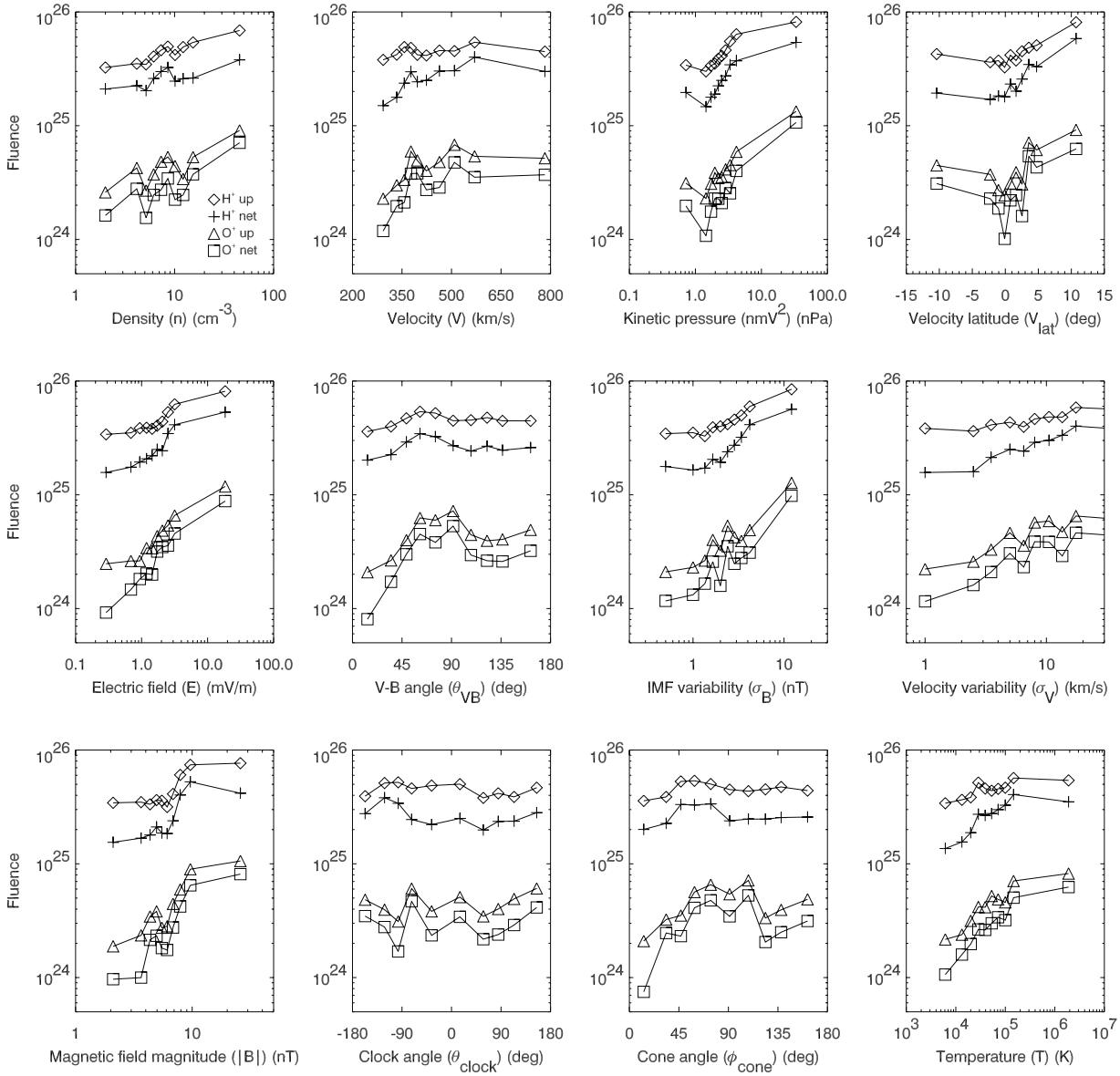

Figure 4. Fluence as a function of various solar wind parameters. The effect of $F_{10.7}$ has been removed using equation (3) to normalize flux values to the mean $F_{10.7}$ value of 114. Both upward fluence and negative net fluence are plotted for each species.

[36] The dependence of fluence on the IMF is examined in the graphs in the bottom row of Figure 4. First, there is a positive correlation with the hourly-averaged magnitude of the magnetic field. As the magnetic and kinetic pressures are highly correlated, this result is perhaps not overly surprising. The next two panels are plots of the fluence versus the clock angle ($\arctan(B_y/B_z)$; positive values in +y direction) and the cone angle (the angle between the IMF and the positive x axis). The sinusoidal dependence on cone angle should also not be particularly surprising given the dependence on electric field: since $\vec{V}$ is typically quite close to the antisunward direction, the cone angle is very similar to θ_{VB}. What is perhaps more interesting is that there is no dependence on the clock angle.

[37] The last graph in Figure 4 is a plot of fluence against solar wind temperature. There is a clear correlation between the two; however, we point out that temperature, like IMF magnitude, is also well-correlated with kinetic pressure.

[38] Some effects might be expected to be moderated or gated by the clock angle. For example, some trends might only occur under northward IMF, or only under southward IMF. To further investigate this, we divided the data into 2 groups: one with clock angle between −45 and 45 degrees, and the other between 135 and 225 degrees. We then reproduced graphs shown in Figure 4, and searched for differences (as might be expected if clock angle acted to moderate or gate other effects). Apart from a slight increase in the magnitude of the cone angle effect for northward IMF, and an overall slightly larger O^+ fluence for southward conditions (consistent with the different *Kp* conditions), we found no differences between the two groups.

Table 1. Correlation Coefficients Between Hour-Averaged Flux and Various Solar Wind Parameters, Normalized by the Maximum Correlation Coefficient Expected for Random Data[a]

Parameter Correlated		R_{corr}/R_{random} Net H^+	Upward H^+	Net O^+	Upward O^+
Solar EUV flux	$F_{10.7}$	**−4.4***	−6.0*	−7.2*	−9.1*
IMF magnitude	$\|B_{IMF}\|$	−3.2	−2.7	−4.5	−5.4
Dst index	Dst	1.9	−2.5	5.5	5.3
IMF variability	σ_B	**−3.8***	−2.3	**−4.1***	−4.5
Kp index	*Kp*	−3.3	0.8	−4.6	−4.8
Pressure	nmv^2	**−2.7***	−2.5	**−3.5***	−3.8*
cos(Velocity latitude)	$\cos(V_{lat})$	**3.6***	3.0*	2.7	3.1
Electric field	E	**−2.0***	−1.5	**−3.9***	−4.8*
Velocity latitude	V_{lat}	**−3.2***	−1.7*	−3.3*	−3.3*
Density	n	−2.4	**−4.1***	−1.8	**−1.8***
Kinetic energy flux	$\frac{1}{2}nmv^3$	**−1.9***	−1.0	**−2.9***	−3.3*
Velocity	V	−0.2	**2.4***	−2.0	−2.5
Temperature	T	−1.1	0.7	−2.2	−2.5
cos(IMF clock angle)	$\cos(\theta_{clock})$	**1.6***	−1.4*	1.5*	0.9
(Electric field)^2	E^2	−0.8	−0.5	−1.8	−2.2
Velocity longitude	V_{long}	−0.8	1.3	−1.0	−1.0
cos(IMF cone angle)	$\cos(\phi_{cone})$	−0.5	0.4	**−1.4***	−1.1
IMF cone angle	ϕ_{cone}	0.4	−0.5	1.3	1.0
cos(V-B angle)	$\cos(\theta_{VB})$	−0.4	0.4	−1.3	−1.0
V-B angle	θ_{VB}	0.3	−0.5	1.2	0.9
sin(IMF clock angle)	$\sin(\theta_{clock})$	0.2	0.3	1.1	1.1
sin(IMF cone angle)	$\sin(\phi_{cone})$	−0.5	−0.4	−0.6	−0.6
cos(Velocity longitude)	$\cos(V_{long})$	0.0	1.2	−0.4	−0.4
sin(V-B angle)	$\sin(\theta_{VB})$	−0.4	−0.4	−0.5	−0.5
IMF clock angle	θ_{clock}	−0.1	−0.4	0.7	0.5
Velocity variability	σ_V	−0.0	0.7	0.2	0.3

[a]Asterisks indicate terms remaining after stepwise multiple regression.

[39] We also investigated the use of different lag times between the solar wind data and the outflow data. Using lags from 5 hours to −1 hour, we replotted Figure 4. None of the graphs was particularly strongly affected, although it should be pointed out that the autocorrelation time of solar wind parameters is long.

7. Multiple Regression Analysis of Solar Wind Dependencies

[40] One way to make an initial assessment of which solar wind parameters might be important is to use the linear correlation coefficient, R, between the solar wind parameters and individual flux measurements. To determine these correlations, we averaged the SMS data into one hour sampling intervals, consistent with the OMNI data, and calculated linear Pearson correlation coefficients between flux values and various solar wind parameters. We list our results, normalized by R_{random} (the maximum absolute value of R expected for two random variables with the same number of data points), in Table 1. At the 95% probability level, $R_{random} = 2/sqrt(N)$ [*Borovsky et al.* [1998] and references therein]. With 7549 data points, R_{random} 0.023, so that even the strongest trends in our data have R values less than 0.3.

[41] The problem with this approach, however, is that it is impossible to separate the causally important parameters from those which are merely correlated with a causally important parameter. For example, is the solar wind temperature important only because of its correlation with pressure? In the absence of an adequate theoretical framework, this question cannot be definitively answered.

[42] There are, however, clues that can be found using multiple regression techniques. In the above case, for example, we can fit two multiple linear models to the data: one including, say, temperature, pressure and $F_{10.7}$, and another without the temperature, and compare the fits using the multiple correlation coefficients R_m. The absolute value of R_m will always be higher for the model with a greater number of parameters, but the two models can be compared with an F test:

$$F = \frac{\left(R_{m1}^2 - R_{m2}^2\right)(N - n - 1)}{\left(1 - R_{m1}^2\right)} \tag{5}$$

where R_{m1} is the R_m value of the test with n terms, R_{m2} is the R_m value of the test with $n - 1$ terms and N is the number of data points. If the value of F is smaller than the cutoff value of the appropriate F-distribution given the number of parameters and the number of data points (at the 95% confidence level), then there is no reason to reject the null hypothesis: that all of the predictive power attributable to the dropped parameter (temperature, in this example) could be explained by the combination of the other parameters and a random variable [*Draper*, 1998]. In other words, there is no reason to keep the parameter.

[43] This forms the basis for what is known as ''backwards elimination stepwise multiple regression''. In this scheme, the data is fit with a multiple linear model using all of the parameters available. The data is then fit using all parameters except one, with the missing parameter cycled through each parameter available. An F test is performed for each fit, and if the lowest F test is below the cutoff, then this single term is eliminated, and the process started over without this parameter. This process is then repeated, eliminating terms one by one, until the F tests indicate that no more terms can be dropped. We performed a stepwise multiple regression on the SMS flux and OMNI data, and have indicated the ''surviving'' terms in Table 1 with asterisks. We did not include *Kp* and Dst, as they are not solar wind variables.

[44] Due to the large number of tests that must be conducted for the above stepwise multiple regression, it is susceptible to Type-2 errors, wherein variables that are not truly related to the flux are identified as such. It is therefore important to use cross-validation of the identified parameters. For the cross-validation, we randomly divided the data into two sets, and performed the tests on each set. We repeated this 1000 times. Although the ''surviving'' terms were not always the same, some patterns emerged in the terms remaining after the elimination:

1. $F_{10.7}$ always remained.
2. Either n, v, or some cross-term of the two, almost always remained.
3. $|E|$ and σ_B frequently remained.
4. $\cos(\theta_{clock})$ occasionally remained, although the magnitude of the regression coefficient was small, and the sign was not constant.
5. V_{lat} almost always remained, although the magnitude of the effect (as seen in the coefficients of the fits) was low.
6. No other terms consistently remained.

[45] Finally, the entire procedure was repeated using lag times between the solar wind measurements and the outflow measurements ranging from 5 hours to −1 hour (not

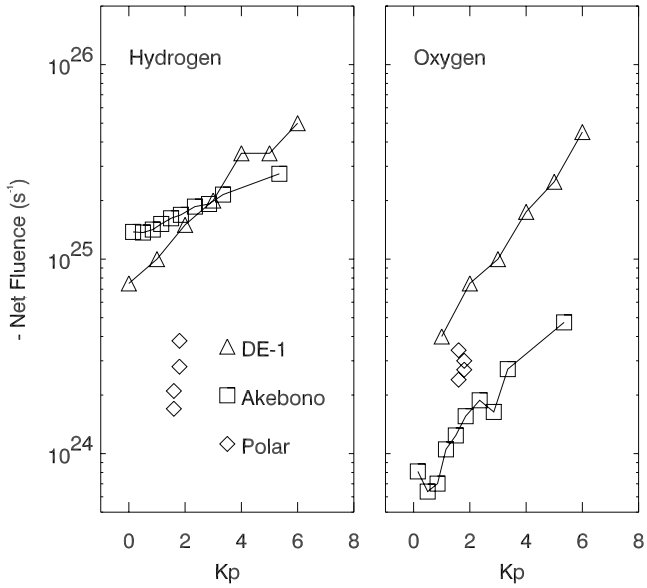

Figure 5. Estimates of hemispheric net ion fluence at solar minimum from various spacecraft at different altitudes (see text). Data from Polar/TIMAS are averages for the season of observation, and are taken from *Peterson et al.* [2001]. DE-1/EICS values are half of the global outflow rates given by *Yau et al.* [1988].

shown). The relations involved remained essentially the same; we attribute this to the long autocorrelation time of the solar wind parameters.

8. Comparison to Other Published Values

[46] Other satellites at similar altitudes which have been used to infer total ion outflow rates include DE-1/EICS [*Yau et al.*, 1988] and Polar/TIMAS [*Peterson et al.*, 2001]. Due to the recent launch date of Polar, only data from solar minimum is available. Figure 5 shows, as a function of *Kp*, total net outflow estimates from DE-1/EICS and Akebono at solar minimum ($70 \leq F_{10.7} < 100$), and from Polar/TIMAS. Polar data from the winter of 1998 are not included, as the average $F_{10.7}$ for that time period is above 100.

[47] The *Kp* value for the Polar measurements was the average over the season of the observation. Due to the exponential dependence of fluence on *Kp*, the "effective" *Kp* is somewhat higher. The altitude ranges used in these studies were 16,000–24,000 km (DE-1), 6000–10,000 km (Akebono) and 6000–8000 km (Polar). Energy ranges were 10 eV–17 keV (DE-1), 1 eV–70 eV (Akebono) and 15 eV–33 keV (Polar). The differences in the energy ranges and altitudes of the instruments make it somewhat difficult to compare the results. Two competing instrumental effects must be considered as the characteristic energy of the distribution increases: ions becoming "visible" after being energized above the low-energy cutoff, and ions becoming "invisible" after being energized above the high-energy cutoff. Energization of the ions as the altitude increases must also be considered.

[48] The poor absolute agreement between Polar/TIMAS and DE-1/EICS is discussed by *Peterson et al.* [2001]. Their interpretation is that Polar does not see a substantial fraction of the polar wind H^+ ions, which are subsequently energized on their way up to DE-1 altitudes and become "visible". The lower energy range of Akebono directly observes this assumed low-energy plasma population, and is in good agreement with the higher-energy observations of DE-1. We interpret this as strongly supporting the explanation of *Peterson et al.* [2001] that the "core" plasma population is accelerated to energies in the DE-1/EICS energy range in the altitude range between 8000 and 20,000 km.

[49] The same comparison for O^+ data leads to a rather different conclusions. Here, Polar/TIMAS estimates agree rather well with DE-1/EICS estimates. *Peterson et al.* [2001] use this to tentatively conclude that "there is little or no thermal above 8000 km". Again, this conclusion is best tested by the current data set, which directly measures this population. The data do, in fact, support this conclusion: fluence estimates from Akebono are much lower than those from either of the other two studies.

[50] The remaining discrepancy between the data sets is the different slopes on the *Kp* trends for H^+ between the DE-1 and Akebono observations. Our interpretation is that as *Kp* increases, the fraction of ions above the SMS detection limit also increases, which tends to reduce the observed slope. On the other hand, since most of the O^+ is above the Akebono energy range, this fraction changes very little, resulting in good agreement on the slope, although poor agreement on the absolute number.

[51] Another comparable study is that of *Lennartsson* [1991, 1995], who used measurements in the tail of O^+ density in the 0.1 to 16 keV range to investigate the dependence of O^+ outflow on solar wind parameters. He found that the O^+ density increased with solar wind ram pressure and electric field, and showed little dependence on B_z polarity. This is precisely in agreement with the observations above (no dependence on σ_B was tested in the Lennartsson studies). In the latter paper, he argued that the electric field dependence (which is emphasized in the earlier paper) may potentially be explained by the mutual correlation of the ram pressure and the electric field, although he concluded that one should "keep an open mind about the exact role of [the electric] field".

9. Discussion

[52] We begin by stressing that while the correlation between ion outflow and any set of solar wind and magnetic activity level parameters is statistically significant, it is also low. This is a point that is sometimes not clearly stated: there is an enormous deviation (frequently more than 3 orders of magnitude) between individual measurements of ion flux and their expected value based on the above trends [see also *Peterson et al.*, 2002]. One attempt to describe this spatial variability of the outflow is discussed in a thesis by *Cully* [2001, electronic version available from the author]; however, this line of research is still in its infancy.

[53] Moreover, it is impossible to establish which solar wind parameters are causally related to ion outflow using a statistical analysis such as this. It is, however, perfectly reasonable to assume that such relations exist, and therefore reasonable to ask which factors are likely to be

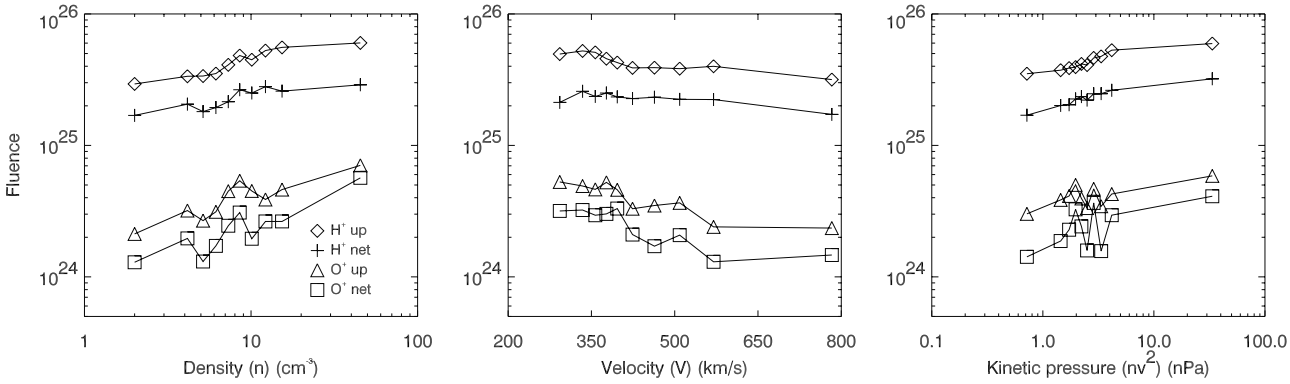

Figure 6. Dependence of ion outflow on density and velocity, in a format similar to Figure 4, after the effects of *Kp* and $F_{10.7}$ have been removed using equation (4).

directly involved. The combination of Figure 4 and the multiple regression analysis performed above leads us to suggest the following solar wind factors as important for consideration:

1. Increased solar wind dynamic pressure is associated with increased ion outflow. This effect has also been seen in studies using Polar [*Moore et al.*, 1999; *Elliott et al.*, 2001].

2. Variability of the IMF (σ_B) is well-correlated with ion outflow. The only similar published result is that of *Moore et al.* [1999], who found a correlation between the ion outflow rate and variation in the solar wind pressure, σ_{mnv^2}. While we do not have data on σ_{mnv^2}, we did find some correlation with σ_v, the variation in the flow velocity. While both σ_B and σ_v correlate well with ion outflow (and also with each other), the correlation was much better between ion outflow and σ_B.

3. Increased solar wind electric field, $|E|$, is associated with increased ion outflow at all locations. This is in agreement with the results of *Lennartsson* [1995] and *Elliott et al.* [2001].

4. The angle between the solar wind flow direction and the GSM equatorial plane (V_{lat}), is well-correlated with the ion outflow. This effect may be due to the yearly variation of V_{lat}, which peaks near the spring equinox. The observed outflow also peaks near the spring equinox, which may be a genuine effect or may be due to statistical biasing of the database due to the 18-month period required to observe all local times.

In contrast, solar wind clock angle seems to have a relatively small effect on outflow. Although this result is in agreement with the results of *Lennartsson* [1995] and *Elliott et al.* [2001], this is still noteworthy, given that the ionospheric convection electric field is highly dependent on this angle.

[54] Concentrating our attention on the 3 parameters mnv^2, σ_B and E, the next important issue is to determine which region of the ionosphere is primarily responsible for the increase in ion outflow. Since in the current work we bin the data by geomagnetic position, this comparison is possible. Comparing the data from the bottom and top quartiles of the distribution of the solar wind parameter, we found that:

1. An increase in E is associated with a latitudinally uniform increase in both net and upward flux. The only notable nonuniformity is that the increase in net flux is somewhat larger on the dayside. The increase in hemispheric outflow (both net and upward) is on the order of 100% for H^+ and 1000% for O^+ (bottom quartile versus top quartile).

2. An increase in σ_B is associated with an increase in hemispheric outflow (both net and upward) on the order of 100% for H^+ and 400% for O^+. The spatial pattern is the same as that seen for changes in E.

3. An increase in pressure is associated with an increase in hemispheric outflow (both net and upward) on the order of 80% for H^+ and 300% for O^+. The increase in upward fluence, and in net H^+ fluence, is relatively uniform, although slightly larger on the nightside. The topography of the net O^+ fluence changes more dramatically. For low pressure, the net fluence is downward between 1500 and 0430 (bins 3,4,7,8 and 10—the region associated by *Lockwood et al.* [1985] with returning downflowing ions from the cleft ion fountain) and upward elsewhere. For high pressure, the net flux is everywhere upward. This is the only grouping where net downward fluences were observed: for both high and low values of σ_B, E and *Kp*, fluences were always upward.

[55] A second, related question is whether the observed trends persist when the effects of *Kp* are removed. We removed the effect of *Kp* in two separate ways: first, we selected data only from limited ranges of *Kp*, and second, we used equation (4) to "normalize" flux values to the same *Kp*. We used both methods, and replotted the graphs in Figure 4. The results were consistent for both techniques: after the removal of *Kp* effects, terms involving solar wind density or velocity dominated, while trends involving other terms were significantly diminished.

[56] O^+ varies with *Kp* much more so than does H^+, so trends in H^+ data were much less affected by the removal of *Kp* than those in O^+. Upward H^+ fluence, in particular, does not vary with *Kp* and was completely unaffected by the process of binning by *Kp*. In general, removing the effect of *Kp* makes the O^+ trends more similar to the H^+ trends. Surprisingly, it also changes the sign of the correlation with solar wind velocity: the correlation of O^+ outflow with velocity, which is positive without binning by *Kp*, becomes negative when binned by *Kp*. This can be seen by comparing Figures 4 (no *Kp* binning) and 6 (with *Kp* binning).

[57] It appears, then, that there are two sets of pathways through which the solar wind energy is transferred to the outflowing ions. The first set of pathways involves the combination of solar wind pressure, electric field and

turbulence. These pathways are associated both with increases in fluence and with increases in *Kp*. The second set of pathways is visible when data is binned by *Kp*. It is a correlation with the solar wind density and an anticorrelation with the solar wind velocity. The change is of a global character, although most pronounced in the dayside low-latitude region (bins 1 and 5).

10. Conclusions

[58] Using a large database of ion observations from the Akebono satellite, we have considered the question "what factors influence the total rate of ion outflow?" by examining two sets of factors: the combination of $F_{10.7}$ and a magnetic activity index (*Kp* in this case), and the combination of $F_{10.7}$ and various solar wind factors. Which of these sets could be viewed as more "fundamental" depends on the problem to which the results are to be applied. Although the predictive performance of *Kp* is better than any of the solar wind parameters, it offers few clues pertaining to the pathways of solar wind energy and momentum through the terrestrial system.

[59] Our examination of $F_{10.7}$ and *Kp* trends extends a known result into the <70 eV energy range of the Akebono/SMS instrument, and addresses for the first time the issue of upward fluence, as distinct from net fluence. This is an important extension; without knowledge of the upward flux, "zero net flux" can mean anything from "no ions present" to "equally large numbers of ions traveling up and down the field line". For H^+, upward and net flux do not respond in the same manner to changing solar wind or *Kp* conditions.

[60] In comparing the hemispheric fluence seen at Akebono with fluences seen by Polar and DE-1, we have confirmed that H^+ is significantly energized in the altitude range between 8000 and 20,000 km, lifting the dominant <10 eV thermal population into the 10 eV to 16 keV energy range. On the other hand, a large part of the O^+ population seen at 8000 km tends to be already energized above 70 eV.

[61] The examination of the solar wind dependence is made difficult by the high degree of collinearity between the solar wind parameters. Nonetheless, we identified four factors as providing sufficient predictive power as to render the other solar wind factors redundant. These factors are: $F_{10.7}$, kinetic pressure, solar wind electric field and variation in the IMF (σ_B). Other solar wind parameters that are well-correlated with these four parameters, and therefore also well-correlated with ion outflow, include the IMF magnitude and cone angle, the solar wind temperature and variation in the solar wind flow speed. The latitudinal orientation of the solar wind flow is also correlated with the outflow rates, although this is likely an artifact of aliasing in the data sampling. It does not appear that the IMF clock angle substantially influences the outflow rate. Our comparisons with solar wind data have been done using hourly averaged data; it is possible that this may hide more complicated relations on a shorter timescale.

[62] The above factors (kinetic pressure, solar wind electric field and σ_B) are associated both with increases in outflow and with increases in *Kp*. When data was grouped by *Kp*, the magnitude of the variation of outflow with each parameter was significantly diminished. We also found two separate relations which are independent of *Kp*: a correlation with the solar wind density and an anticorrelation with the solar wind velocity. When data from all levels of *Kp* are used, these relations are masked by the larger variation with kinetic pressure. This may point to a separate pathway through which solar wind energy is coupled more directly to ion outflow, although we offer no explanation of the underlying mechanism(s) responsible.

[63] With a better understanding of how ion outflow is associated with solar wind conditions, it also becomes possible to assess the ionospheric contribution farther out into the magnetosphere. In a companion paper [*Cully et al.*, 2003], we use the region specific upward fluence from this study as input for a Monte Carlo simulation of ion outflow. The objective of this second study is to quantify the supply of ions of ionospheric origin to the CPS.

[64] **Acknowledgments.** We acknowledge K. W. Ogilvie and A. J. Lazarus for their contributions to the OMNIweb database of the National Space Science Data Center (NSSDC), and the efforts of the NSSDC in maintaining the OMNIWeb database, time shifting of the OMNIWeb data, and the provision of excellent documentation. Support for this research was provided by the Canadian Space Agency and the Natural Sciences and Engineering Research Council of Canada. CMC was also supported by the Alberta Heritage Scholarship fund. We thank the members of the Akebono Science Team for their cooperation in the Akebono science operation.

References

Abe, T., B. Whalen, A. Yau, R. Horita, S. Watanabe, and E. Sagawa, EXOS-D (Akebono) SMS observations of the polar wind, *J. Geophys. Res.*, *98*, 11,191–11,203, 1993.

Abe, T., S. Watanabe, B. A. Whalen, A. W. Yau, and E. Sagawa, Observations of polar wind and thermal ion outflow by Akebono/SMS, *J. Geomagn. Geoelectr.*, *48*, 319–325, 1996.

André, M., and A. Yau, Theories and observations of ion energization and outflow in the high latitude magnetosphere, *Space Sci. Rev.*, *80*, 27–48, 1997.

Borovsky, J. E., M. F. Thomsen, and R. C. Elphic, The driving of the plasma sheet by the solar wind, *J. Geophys. Res.*, *103*, 17,617–17,639, 1998.

Chandler, M., J. Waite, and T. Moore, Observations of polar ion outflows, *J. Geophys. Res.*, *96*, 1421–1428, 1991.

Chandler, M. O., Observations of downward moving O^+ in the polar topside ionosphere, *J. Geophys. Res.*, *100*, 5975, 1995.

Chappel, C. R., T. E. Moore, and J. H. Waite Jr., The ionosphere as a fully adequate source of plasma for the earth's magnetosphere, *J. Geophys. Res.*, *92*, 5896–5910, 1987.

Cully, C. M., Observations and trajectory simulations of terrestrial ion outflow, Master's thesis, Univ. of Calgary, Alberta, Canada, 2001.

Cully, C. M., E. F. Donovan, A. W. Yau, and H. J. Opgenoorth, Supply of ionospheric ions to the central plasma sheet, *J. Geophys. Res.*, *108*, doi:10.1029/2002JA009457, in press, 2003.

Delcourt, D. C., C. R. Chappell, T. E. Moore, and J. H. Waite Jr., A three-dimensional numerical model of ionospheric plasma in the magnetosphere, *J. Geophys. Res.*, *94*, 11,893–11,920, 1989.

Drakou, E., A. Yau, and T. Abe, Ion temperature measurements from the Akebono suprathermal mass spectrometer: Application to the polar wind, *J. Geophys. Res.*, *102*, 17,523–17,539, 1997.

Draper, N. R., *Applied Regression Analysis*, *Wiley Ser. Probab. Math. Stat.*, 3rd. ed., John Wiley, New York, 1998.

Elliott, H. A., R. H. Comfort, P. Craven, M. O. Chandler, and T. E. Moore, Solar wind influence on the oxygen content of ion outflow in the high-altitude polar cap during solar minimum conditions, *J. Geophys. Res.*, *106*, 6067–6084, 2001.

Hultqvist, B., M. Øieroset, G. Paschmann, and R. Treumann, Magnetospheric plasma sources and losses. Final report of the ISSI study project on source and loss processes of magnetospheric plasma, *Space Sci. Rev.*, *88*, 1, 1999.

Lennartsson, O. W., Statistical investigation of IMF B_z effects on energetic (0.1 to 16-keV/e) magnetospheric O^+ ions, *J. Geophys. Res.*, *100*, 23,621–23,635, 1995.

Lennartsson, W., Solar control of the Earth's emission of energetic O^+, *J. Atmos. Terr. Phys.*, *53*, 1103–1111, 1991.

Lockwood, M., M. O. Chandler, J. Horwitz, J. J. H. Waite, T. E. Moore, and C. R. Chappel, The cleft ion fountain, *J. Geophys. Res.*, *100*, 9736–9748, 1985.

Miyake, W., T. Mukai, and N. Kaya, Interplanetary magnetic field control of dayside ion conics, *J. Geophys. Res.*, *105*, 23,339, 2000.

Moore, T., et al., Ionospheric mass ejection in response to a CME, *Geophys. Res. Lett.*, *26*, 2339, 1999.

Norqvist, P., M. André, and M. Tyrland, A statistical study of ion energization mechanisms in the auroral region, *J. Geophys. Res.*, *103*, 23,459–23,473, 1998.

Øieroset, M., M. Yamauchi, L. Liszka, and B. Hultqvist, Energetic ion outflow from the dayside ionosphere: Categorization, classification, and statistical study, *J. Geophys. Res.*, *104*, 24,915, 1999.

Peterson, W. K., H. L. Collin, A. W. Yau, and O. W. Lennartsson, Polar/Toroidal Imaging Mass-Angle Spectrograph observations of suprathermal ion outflow during solar minimum conditions, *J. Geophys. Res.*, *106*, 6059–6066, 2001.

Peterson, W. K., H. L. Collin, M. Boehm, A. W. Yau, C. Cully, and G. Lu, Investigation into the spatial and temporal coherence of ionospheric outflow on January 9–12, 1997, *J. Atmos. Sol. Terr. Phys.*, *64*(15), 1659–1666, 2002.

Su, Y.-J., J. Horwitz, T. Moore, B. Giles, M. Chandler, P. Craven, M. Hirahara, and C. Pollock, Polar wind survey with the Thermal Ion Dynamics Experiment/Plasma Source Instrument suite aboard Polar, *J. Geophys. Res.*, *103*, 29,305, 1998.

Whalen, B., et al., The Suprathermal ion Mass Spectrometer (SMS) onboard the Akebono (EXOS-D) satellite, *J. Geomagn. Geoelectr.*, *42*, 511–536, 1990.

Yau, A., and M. André, Sources of ion outflow in the high latitude ionosphere, *Space Sci. Rev.*, *80*, 1–25, 1997.

Yau, A., E. Shelley, W. Peterson, and L. Lenchyshyn, Energetic auroral and polar ion outflow at DE 1 altitudes: Magnitude, composition, magnetic activity dependence, and long-term variations, *J. Geophys. Res.*, *90*, 8417–8432, 1985.

Yau, A., E. Drakou, M. Greffen, D. Knudsen, and E. Sagawa, Radio-frequency ion mass spectrometer measurements of ion composition, velocity, and temperature: The EXOS-D suprathermal mass spectrometer, in *Measurement Techniques in Space Plasmas: Particles*, *Geophys. Monogr. Ser.*, vol. 102, edited by R. F. Pfaff et al., pp. 307–312, AGU, Washington, D. C., 1998.

Yau, A. W., W. K. Peterson, and E. G. Shelley, Quantitative parameterization of energetic ionospheric ion outflow, in *Modeling Magnetospheric Plasma*, *Geophys. Monogr. Ser.*, vol. 44, edited by T. E. Moore and J. H. Waite Jr., p. 211, AGU, Washington, D. C., 1988.

G. G. Arkos, C. M. Cully, E. F. Donovan, and A. W. Yau, Department of Physics and Astronomy, University of Calgary, Calgary, Alberta, Canada T2N 1N4. (cully@phys.ucalgary.ca; eric@phys.ucalgary.ca; yau@phys.ucalgary.ca)